Nucleic Acids Research, 2025, **53**, gkaf190
https://doi.org/10.1093/nar/gkaf190
Genome integrity, repair and replication

A conserved thumb domain insertion in DNA polymerase epsilon supports processive DNA synthesis

Sohail Ahmad[†], **Siying Zhang**[†], **Xiangzhou Meng**[*]

State Key Laboratory of Microbial Metabolism, and School of Life Sciences & Biotechnology, Shanghai Jiao Tong University, Shanghai 200240, China

[*]To whom correspondence should be addressed. Email: mengx@sjtu.edu.cn
[†]The first two authors contributed equally to this work.

Abstract

The leading strand DNA polymerase, Pol ε, plays a crucial role in DNA replication and maintenance of genome stability. In contrast to other replicative polymerases, Pol ε contains unique structural domains that likely underlie its specialized functions. However, the contribution of these structural elements to the functional capabilities of Pol ε remain poorly understood. In this study, we identify a conserved thumb domain insertion as a key determinant of the processivity of Pol ε in *Saccharomyces cerevisiae*. Disruption of this insertion leads to genome instability and significant defects in DNA replication. *In vitro* DNA binding and polymerase assays demonstrate that this insertion is critical for tight DNA binding and efficient processive synthesis. Our results highlight the essential role of this previously uncharacterized thumb domain insertion in supporting the intrinsic processivity of Pol ε.

Graphical abstract

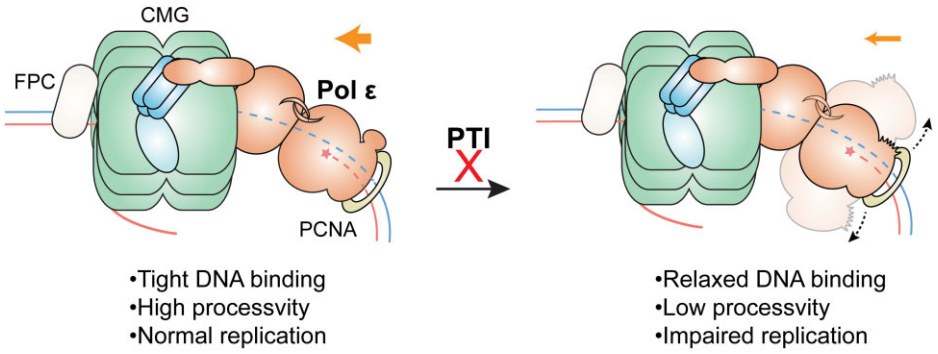

Introduction

Faithful genomic duplication in eukaryotes requires high-fidelity DNA polymerases to accurately replicate DNA from templates. Three highly conserved B family DNA polymerases are responsible for synthesizing nuclear DNA [1, 2]. DNA polymerase alpha (Pol α)-primase initiates RNA-DNA primers, while DNA polymerase epsilon (Pol ε) and DNA polymerase delta (Pol δ) synthesize the bulk of the leading strand and lagging strand DNA, respectively [3–5].

Pol ε consists of four subunits: Pol2, Dpb2, Dpb3, and Dpb4 in budding yeast [6–8]. The catalytic subunit, Pol2, is divided into two halves: the *N*-terminal half (Pol2N) and the C-terminal half (Pol2C). Pol2N contains both the polymerase and exonuclease domains, which are responsible for adding nucleotides and removing mis-incorporated ones on the growing nascent strand. The polymerase domain can be further divided into the palm, fingers and thumb domains. The palm domain binds to the extendable end of the DNA and contains the active site that catalyzes the nucleotidyl transferase reaction, while the fingers are involved in positioning the incoming complementary dNTP through conformational change [9–11]. The thumb domain primarily interacts with the double-stranded part of the template-primer DNA. Pol2N corresponds to Pol3, the catalytic subunit of Pol δ. Deletion of Pol2N causes cell sickness, but not lethality, as Pol δ can inefficiently synthesize leading strand DNA [12–14].

Conversely, Pol2C is indispensable. As the second polymerase-exonuclease module of Pol2, Pol2C has evolved to become inactivated and gain new functions [15]. Pol2C, in collaboration with Dpb2, plays a vital role in assembling the active replicative helicase CMG (Cdc45-Mcm2-7-GINS) complex and in origin firing [16–20]. Moreover, Pol2C is

Received: September 14, 2024. **Revised:** February 20, 2025. **Editorial Decision:** February 24, 2025. **Accepted:** February 26, 2025

responsible for checkpoint activation in response to replication stress [21, 22]. Dpb3 and Dpb4, which are non-essential subunits of Pol ε, play a key role in depositing parental histone H3-H4 onto leading strand DNA during replication [23]. Additionally, Dpb3 and Dpb4 bind to double-stranded DNA and support processive DNA synthesis by Pol ε [24, 25]. A recent study on Pol ε holoenzyme structure revealed that Dpb3-Dpb4 bridges the Pol2N and Pol2C modules to form a rigid holoenzyme [8].

Processive DNA synthesis by both leading and lagging strand polymerases relies on the proliferating cell nuclear antigen (PCNA) [26–32]. PCNA is a ring-shaped, homotrimeric sliding clamp that encircles and slides along the nascent double-stranded DNA, thereby enhancing the processivity of replicative DNA polymerases. Previous studies in budding yeast have shown that Pol ε and Pol δ exhibit comparable processivity in the presence of PCNA [29]. However, compared to Pol δ, Pol ε has a lower binding affinity to PCNA and is less stimulated by it; nevertheless, Pol ε displays a much higher binding affinity to DNA and possesses significantly higher intrinsic processivity [9, 29]. This elevated intrinsic processivity is primarily supported by unique domains within the Pol2N of Pol ε.

One such domain, the P domain, has been shown to facilitate the encirclement of the nascent DNA duplex by Pol ε and is essential for its high processivity *in vitro* [9]. Another unique domain of Pol2N, known as the POPS domain, is positioned at the outer edge of the catalytic domain and supports replication progression by balancing the polymerase and exonuclease activities of Pol ε [33, 34]. SUMOylation of the POPS domain during S phase or under replication stress further enhances replication efficiency [35]. Despite these well-documented domains, there are additional conserved structural insertions specific to the Pol2/POLE family, the functions of which remain unknown. Investigating these insertions is crucial for fully understanding the biological role of Pol ε.

In this study, we investigated a previously uncharacterized thumb domain insertion specific to Pol ε. We demonstrate that deletion or mutation of this insertion in yeast cells leads to growth retardation, delayed S phase progression, and genomic instability. More importantly, we found a defect in replication progression in the mutant cells. *In vitro* DNA polymerase activity and DNA binding assays suggest that this thumb domain insertion supports progressive DNA replication by promoting tight binding of the DNA polymerase domain to the DNA substrate.

While preparing our manuscript, cryo-electron microscopy structures of human Pol ε-PCNA were reported, revealing that the human counterpart of this thumb domain insertion forms one of the interaction interfaces with PCNA [11, 36]. However, the interface is minimal, and its functional significance remains unexplored. The primary PCNA-interacting motif of Pol ε, in both budding yeast and humans, is the PCNA-interacting peptide (PIP) box [11, 31, 36, 37]. Our study shows that mutations in the PIP box result in a milder phenotype compared to mutations in the thumb domain insertion. This suggests that the importance of this insertion extends beyond its interaction with PCNA, even if the interaction is indeed functional in budding yeast. Finally, we conclude that this thumb domain-specific insertion of Pol ε plays a crucial role in maintaining the intrinsic processivity of Pol ε.

Materials and methods

Yeast strains and genetic manipulation

Yeast strains, originating from W1588-4C, a *RAD5* variant of W303 (*MATa ade2-1 can1-100 ura3-1 his3-11,15 leu2-3*, and *112 trp1-1 rad5-535*) [38], are detailed in Supplementary Table S1. Each experiment assessed at minimum of two strains per genotype, with only one strain listed per genotype. Gene mutations, deletions, and protein tag insertions at endogenous loci were achieved using CRISPR-Cas9 genome editing and one-step replacement employing marker cassettes. Standard PCR-based methods were used for DNA cloning, followed by sequence confirmation.

Cell cycle arrest, release and flow cytometry analysis

Yeast cell G1 arrest and release followed a standard protocol. Log-phase cultures were treated with alpha-factor (5 μg/ml) until >90% of cells arrested in G1. Samples were collected at various time points post double washes and release in YPD medium. Flow cytometry analyses adhered to a standard procedure. Ethanol-fixed yeast cells underwent washing and resuspension in a sodium citrate solution. Subsequent removal of RNAs and proteins involved successive additions of RNase A and Proteinase K. DNA was stained with Sytox Green. Flow cytometry utilized a CytoFlex flow cytometer (BECKMAN COULTER), with data analysis performed using FlowJo.

GCR and mutation rate assays

The GCR assay followed a standard protocol, and rates were calculated [39, 40]. The *URA3-CAN1* cassette was inserted at YEL068c. At least ten cultures were tested for each genotype. To determine the number of colonies that lose the *URA3-CAN1* cassette and the total viable colonies, cells were plated on SC + 5-FOA + canavanine (FC) and YPD plates, respectively. The GCR rates were computed as m/NT, where m(1.24 + ln[m]) - NFC = 0 and m represents mutational events, NFC represents the number of colonies on FC plates, and NT represents colonies that formed on YPD plates. Mutation rates were determined using the fluctuation assay [41]. Briefly, an overnight culture was diluted (1:10 000) and 100 μl of the diluted culture was distributed into each well of a 96-well plate. The plate was incubated at 30°C until cultures reached saturation. Twenty-four of the cultures were combined, diluted and plated on YPD plates for total cell number (N) calculation. The remaining 72 cultures were plated on SC + canavanine plates for mutation events per culture (m) calculation. Mutation rates were calculated using the Ma–Sandri–Sarkar maximum likelihood method, and 95% confidence intervals were calculated.

Two-dimensional agarose gel electrophoresis

Genomic DNA extraction followed a standard cetyltrimethylammonium bromide (CTAB) protocol [42]. Initially, yeast cells were treated with zymolyase to generate spheroplasts. Subsequently, after cell lysis and proteinase K treatment to degrade proteins, DNA was extracted and precipitated by CTAB. DNA digestion, and two-dimensional (2D) gel running, and DNA transfer were performed according to previously established procedures [33]. For southern blot analysis, a biotin-labeled DNA probe was used for hybridization, followed by chemiluminescent detection using

a kit (Thermo Fisher Scientific, Cat. # 89 880). Two origins ARS305 and ARS1212 were probed.

Co-immunoprecipitation and western blotting

To get whole-cell extract (WCE), cells were lysed by bead-beating in lysis buffer, followed by nucleic acid digestion with Benzonase and centrifugation 15 000 rpm for 20 min. For investigating the level of the CMG complex, the lysis buffer composition included 100 mM HEPES-KOH pH 7.5, 100 mM potassium acetate, 10 mM magnesium acetate, 0.1% NP-40, 2 mM EDTA-KOH pH 8.0, 2 mM β-glycerophosphate, 2 mM sodium fluoride, 1 mM DTT, 1 mM PMSF, 10 μg/ml leupeptin, 1 μg/ml pepstatin A, 10 mM benzamidine HCl, and 1 × protease inhibitor cocktail (APExBIO, Cat. # K1009). For co-immunoprecipitation of Pol2 and Dpb2, the lysis buffer contained 50 mM HEPES-KOH pH 7.5, 140 mM sodium chloride, 1% Triton X-100, 2 mM magnesium chloride, 2 mM β-glycerophosphate, 2 mM sodium fluoride, 1 mM DTT, 1 mM PMSF, 10 μg/ml leupeptin, 1 μg/ml pepstatin A, 10 mM benzamidine HCl, and 1x protease inhibitor cocktail (APExBIO, Cat. # K1009). WCE was then incubated with Flag or Myc antibody plus Protein G beads for 3 h at 4°C. Proteins bound to the beads were washed and then eluted with 2 × Laemmli buffer without DTT. Protein samples were boiled prior to SDS-PAGE and transferred to nitrocellulose membrane for western blotting analysis. The antibodies employed include anti-Flag (Smart-Lifesciences #SLAB0102), anti-Myc (Smart-Lifesciences #SLAB2903), anti-HA (Smart-Lifesciences #SLAB0202), anti-β-Tubulin (ShareBio #SB-AB0039), and anti-Rad53 (Abcam #ab104232).

Protein purification

The proteins used in the polymerase assay, exonuclease activity assay and EMSA were homogeneously purified following a standard protocol with some modifications [43]. Protein quantification was performed using the Bradford method.

Pol ε

Cells harboring constructs for galactose-inducible Pol ε^{WT} or Pol ε^{6A} were cultured at 30°C in YP-GL (YP + 2% glycerol/2% lactic acid) to a density of 2–4 × 10^7 cells/ml. Galactose induction (2%) was initiated, and cells were grown for 4 h. Subsequently, cells were harvested by centrifugation and washed once with 1 M sorbitol/25 mM HEPES-KOH pH 7.6, followed by a second wash with buffer A (45 mM HEPES-KOH pH7.6, 0.02% NP40, 10% glycerol)/100 mM NaCl. Cell pellet was resuspended in 0.5 × volume of Buffer A/100 mM NaCl/1 mM DTT/protease inhibitors, then frozen dropwise in liquid nitrogen. The resulting popcorn was crushed in Mixer Mill MM 400 (Retsch) for two cycles of 4.5 min at maximum power. Crushed cell powder was resuspended in 1 volume of Buffer A/100 mM NaCl/1 mM DTT. The final NaCl concentration was adjusted to 0.3 M, and the lysate was centrifuged at 23 000 rpm for 1 h to remove debris. The soluble extract was supplemented with 2 mM $CaCl_2$ and incubated for 3 h at 4°C with calmodulin resins. The beads were washed with Buffer A/300 mM NaCl/2 mM $CaCl_2$/1 mM DTT. Bead-bound proteins were eluted with Buffer A/300 mM NaCl/1 mM EDTA/2 mM EGTA/1 mM DTT. Eluates from affinity purification were dialyzed in Buffer A/150 mM NaCl/1 mM DTT and then fractionated on a Mono Q 5/50 GL column with a salt gradient of 150–500mM NaCl. MonoQ peak fractions were concentrated and fractionated by gel filtration using the Superdex^{TM}-200 column in Buffer A/300mM KOAc/1 mM DTT.

PCNA

The pET28a-His-PCNA plasmid was transformed into BL21(DE3) cells. Cultures were grown at 37°C until an OD_{600} of 0.5 was reached, then induced with 0.5 mM IPTG at 20°C overnight. Cells were harvested by centrifugation at 4000 rpm for 20 min. The cell pellet was resuspended in lysis buffer (50 mM Na-phosphate pH 7.6/400 mM NaCl/10 mM imidazole/1 mM DTT) /protein inhibitors, and lysed by sonication. The lysate was centrifuged at 18 000 rpm for 1 h to remove cell debris. The supernatant was incubated with Ni NTA beads for 2 h at 4°C. The beads were washed with 10 CV of lysis buffer, followed by 2CV of lysis buffer containing 50 mM imidazole. Proteins were eluted with a gradient of imidazole: 2 CV with 100 mM, 8 CV with 150 mM, 5 CV with 300 mM imidazole in lysis buffer. Eluates were dialyzed against 25 mM Tris HCl pH 7.5/1 mM EDTA/10% glycerol/0.1 M NaCl/1 mM DTT, then fractionated on a Mono Q 5/50 GL column with a salt gradient of 0.1–1 M NaCl. The peak fractions were further purified using a Superdex 200 column equilibrated in 25 mM HEPES-KOH pH 7.6/300 mM K-acetate/1 mM EDTA/10% glycerol/1 mM DTT.

RFC

Cells harboring constructs for galactose-inducible RFC were cultured at 30°C in YP-GL (YP + 2% glycerol/2% lactic acid) to a density of 2–4 × 10^7 cells/ml. Expression was induced with 2% galactose at 30°C for 3 h. Cells were harvested by centrifugation at 4000 rpm for 20 min and washed twice, first with 1 M sorbitol/25 mM HEPES-KOH pH 7.6 and then with 25 mM Tris-HCl pH 7.5/10% glycerol/100 mM NaCl. The cell pellet was resuspended in 25 mM Tris-HCl pH 7.5/10% glycerol/100 mM NaCl/1 mM DTT/protease inhibitors, then frozen dropwise in liquid nitrogen. The resulting popcorn was crushed in Mixer Mill MM 400 (Retsch) for 2 cycles of 4.5 min at maximum power. Crushed cell powder was resuspended in 1 volume of 25 mM Tris-HCl pH 7.5/10% glycerol/0.02% NP-40/100 mM NaCl/1 mM DTT. The final NaCl concentration was adjusted to 0.4 M, and the lysate was centrifuged at 23 000 rpm for 1 h to remove debris. The supernatant was incubated with anti-FLAG resin for 2 h at 4°C. The resin was washed with 25 mM Tris-HCl pH 7.5/10% glycerol/300 mM NaCl/1 mM DTT, and proteins were eluted with 25 mM Tris-HCl pH 7.5/10% glycerol/300 mM NaCl/0.5 mg ml^{-1} 3 × FLAG peptide. Eluates were dialyzed against 25 mM Tris-HCl pH 7.5/10% glycerol/100 mM NaCl/1 mM DTT, then fractionated on a Mono Q 5/50 GL column with a salt gradient of 0.1–1 M NaCl.

RPA

The pJM126 was transformed into BL21(DE3) cells [44]. Cultures were grown at 37°C until an OD_{600} of 0.2 was reached, then shifted to 17°C and grown to an OD_{600} of 0.5. Expression was induced with 0.4 mM IPTG at 30°C for 4 h. Cells were harvested by centrifugation at 4000 rpm for 20 min. The cell pellet was resuspended in 0.5 × volume of 25 mM Tris HCl pH 7.5/1 mM EDTA/10% glycerol/1 M NaCl/1 mM DTT/protease inhibitors/0.1 mg/ml lysozyme, then lysed by sonication. The lysate was centrifuged at 23 000 rpm for 30 min to remove debris. The supernatant was adjusted to a final

NaCl concentration of 0.5 M and applied to a Hitrap blue column. The column was washed with 10 CV of 25 mM Tris-HCl pH 7.5/1 mM EDTA/10% glycerol/0.5 M NaCl /1 mM DTT, followed by 10 CV of 25 mM Tris-HCl pH 7.5/10% glycerol/0.02% NP-40/0.8 M NaCl/1 mM DTT. Proteins were eluted with 10 CV of 25 mM Tris-HCl pH 7.5/1 mM EDTA/10% glycerol/2.5 M NaCl/1 mM DTT/40% ethylene glycol. Peak fractions were combined, adjusted to 0.5 M NaCl, and incubated with ssDNA cellulose (Worthington) for 1 h at 4°C. The column was washed with 2 CV of 25 mM Tris-HCl pH 7.5/1 mM EDTA/10% glycerol/0.5 M NaCl/1 mM DTT, followed by 2 CV of 25 mM Tris-HCl pH 7.5/1 mM EDTA/10% glycerol/0.8 M NaCl/1 mM DTT. Proteins were eluted with 5 CV of 25 mM Tris-HCl pH 7.5/1 mM EDTA/10% glycerol/1.5 M NaCl/1 mM DTT/50% ethylene glycol. Eluates were dialyzed against 25 mM Tris-HCl pH 7.5/1 mM EDTA/10% glycerol/0.1 M NaCl/1 mM DTT, then fractionated on a Mono Q 5/50 GL column with a salt gradient of 0.15–1 M NaCl.

In vitro DNA polymerase and exonuclease assays

The DNA polymerase activity and exonuclease activities with short oligonucleotide substrates were measured using established protocols with slight modifications [45,46]. Substrates for these assays were prepared by annealing 5′ Cy5- or FAM-labeled 50-nt oligonucleotide to an 80-mer template. The annealing process was conducted by incubating the primer and template in a 1:1 ratio with 150 mM sodium acetate at 92°C for 2 min, followed by gradual cooling to room temperature over ∼2 h. For the polymerase assay, the reaction mixture contained the following components: 40 mM Tris-HCl (pH 7.8), 125 mM sodium acetate, 8 mM magnesium acetate, 1 mM DTT, 0.2 mg ml^{-1} bovine serum albumin (BSA), 30 μM dCTP, 80 μM dTTP, 38 μM dATP, 26 μM dGTP, 25 nM oligonucleotide substrate, and Pol ε at the designated concentration. For the exonuclease assay, the reaction mixture contained the same buffer composition except for the omission of dNTPs. Both reactions were incubated at 30°C for 10 min, with samples collected at designated time points. Reactions were quenched by adding an equal volume of 2 × loading buffer (95% deionized formamide, 25 mM EDTA, Orange G). Samples were subjected to electrophoresis on a 10% denaturing polyacrylamide gel containing 8 M urea in 1 × TBE buffer. Quantification was performed using a Typhoon fluorescence imaging system (GE Healthcare).

For the polymerase assay involving a long template, protocols were based on previous studies [29, 46] with modifications. Specifically, a 5′ Cy5-labeled 50-nt oligonucleotide was annealed to M13mp18 ssDNA in a 1:1 ratio by heating at 92°C for 5 min, followed by gradual cooling to room temperature. The primer extension reactions were conducted in a buffer containing 40 mM Tris-HCl (pH7.8), 125 mM NaAc, 8 mM magnesium acetate, 1 mM DTT, 0.2 mg ml^{-1} BSA, 1 mM ATP, 100 μM dNTPs, and 1.5 nM DNA template. Initially, 600 nM RPA was added and incubated at 30°C for 5 min. The mixture was then divided into two groups: one group received 15 nM RFC and 37.5 nM PCNA, while the other group received 15 nM RFC only. Both groups were incubated at 30°C for 5 min, followed by the addition of 3.75 nM Pol ε^{WT} or Pol ε^{6A} to initiate replication. Samples (50 μl) were collected at 0, 7.5, 15 min, and reactions were quenched by adding 10 μl of stop solution (250 mM EDTA, 1% SDS). Proteinase K (10 μl of 20 mg ml^{-1}) was added to the samples, which were incubated at 55°C for 1 h. DNA was purified by phenol/chloroform extraction, washed, and resuspended. A 6 × alkaline loading buffer (300 mM NaOH, 6 mM EDTA, 18% Ficoll, 0.15% bromocresol green, 0.25% xylene cyanol) was added to each sample. Replication products were separated on a 0.8% alkaline agarose gel, and quantification was performed using a Typhoon fluorescence imaging system (GE Healthcare).

All oligonucleotides used in the in vitro polymerase or exonuclease assays are listed in Supplementary Table S2.

Electrophoretic mobility shift assay

Purified Pol ε^{WT} and Pol ε^{6A} proteins were pre-mixed with 5′FAM-labeled DNA substrates as used in the polymerase assay. Various concentration of Pol ε (1, 2, 5, 7.5, and 10 nM) were tested with a fixed DNA concentration of 25 nM in a buffer containing 20 mM HEPES (pH 7.6), 10% glycerol, 2 mM EDTA, 2 mM DTT, 0.2 mg ml^{-1} BSA, and 0.02% NP-40. Binding was carried out for 25 min at 4°C. Subsequently, 5 × loading buffer (50% glycerol, 0.025% Orange G) was added, and the protein-DNA complexes were resolved by 4% polyacrylamide gel electrophoresis at 100 V for 30 min at 4°C in 1 × TGE buffer. Quantification was performed using a Typhoon fluorescence imaging system (GE Healthcare).

Results

A thumb domain insertion is crucial for cell growth

It has been previously reported that there is a Pol2/POLE specific insertion in the thumb domain (residues 1116–1140 of yeast Pol2), consisting of two α-helices and a coil region in between (Fig. 1A) [9]. This domain, referred to as PTI (Polymerase Thumb domain Insertion), is conserved across eukaryotes and absent in other replicative polymerases, suggesting its functional importance (Fig. 1A). To assess the significance of this region, we initially generated and examined a full-length deletion mutant (Fig. 1B, PTI: A). While complete deletion of this insertion does not result in lethality, the mutant exhibits severe growth defects, indicating the critical role of this region in Pol ε function (Fig. 1C, *pol2-ΔPTI_A*). We further generated partial deletions of this domain to identify the major responsive region (Fig. 1B). Our findings reveal that deletion of a small region consisting of six amino acids (residues 1131–1136) in the coil region leads to growth defects similar to those observed with the full region deletion, whereas deletion of either α-helix has minimal impact on cell growth (Fig. 1C and D).

Western blotting analysis of total protein extracted from yeast cells showed no significant changes in Pol ε protein levels among these deletion mutants, suggesting that the growth defects primarily result from disruption of PTI function rather than a reduction in Pol ε protein levels (Supplementary Fig. S1). Additionally, we investigated the association of Dpb2 and Pol2 using coimmunoprecipitation to determine whether it is affected in the mutant *pol2-PTI (1131–1136) Δ* (abbreviated as *pol2-6Δ*). Our results indicate no changes in Pol2-Dpb2 association in *pol2-6Δ* compared with the wild-type (Fig. 1E). In conclusion, our findings demonstrate the crucial role of PTI in Pol ε for cell growth, highlighting its functional importance.

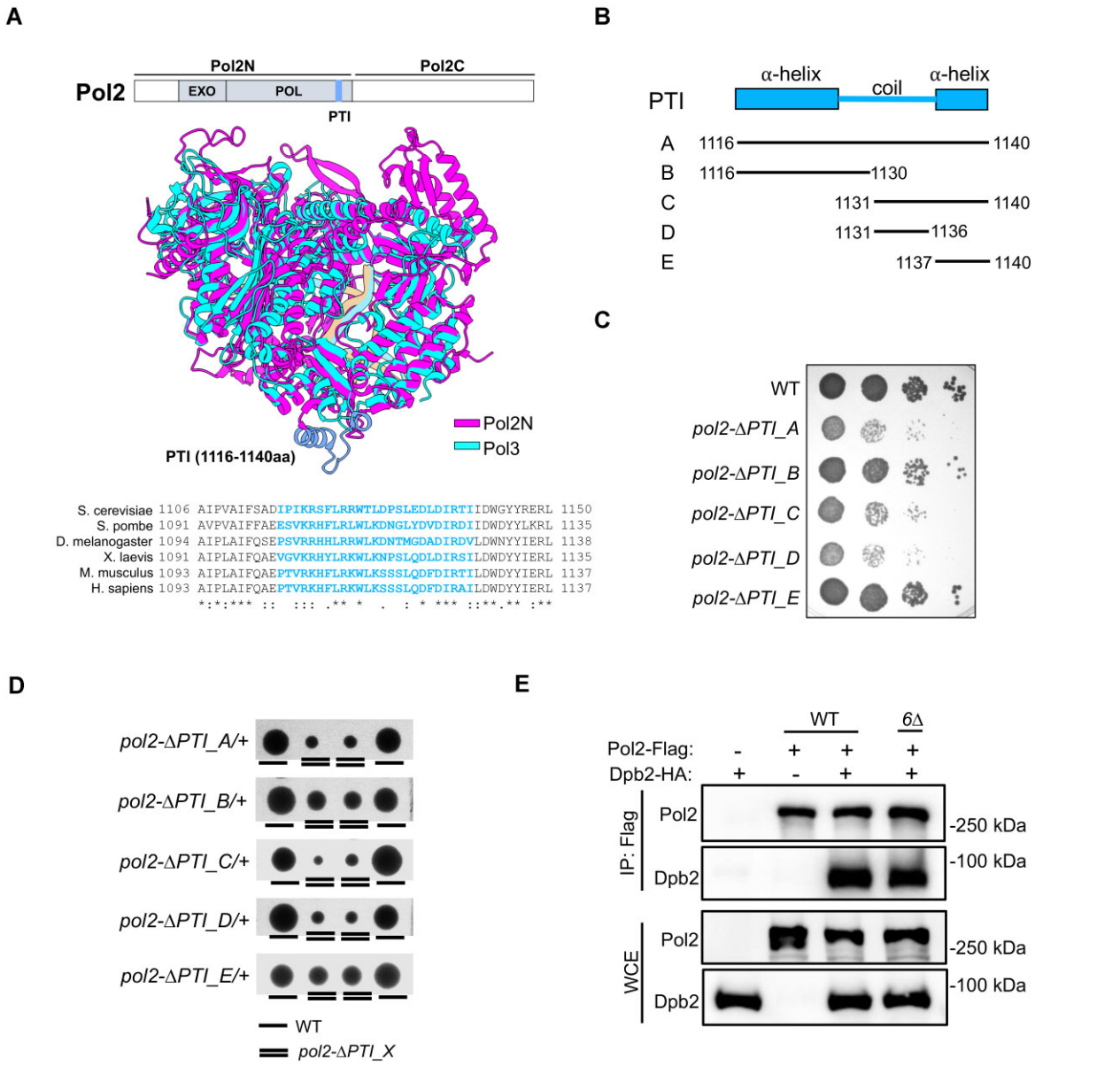

Figure 1. Mutating Pol2-PTI impairs cell growth. (**A**) Top: Schematic of Pol2 domain organization. EXO: Exonuclease domain, POL: Polymerase domain, PTI: Polymerase thumb domain insertion. Middle: Superimposition of the crystal structure of Pol2 *N*-terminal half (PDB: 4M8O) with that of budding yeast Pol3 (PDB: 3IAY). The PTI domain is highlighted. Bottom: Sequence alignment of the PTI domain in various eukaryotic species using Clustal Omega. Symbols "*," ":," and "." indicate a fully conserved residue, conservation between groups of strongly similar properties, and conservation between groups of weakly similar properties, respectively. (**B**) Schematic representation of different deletion mutations of PTI. (**C**) Wild-type, and different PTI deletion mutant cells were spotted at 10-fold serial dilutions on YPD medium and incubated at 24°C for 3 days. (**D**) Heterozygous diploid cells with various PTI deletion mutations were subjected to tetrad analysis on YPD medium, and incubated at 24°C for 3 days. (**E**) Analysis of Pol2 association with Dpb2 in *pol2-ΔPTI_D (pol2-6Δ)* strain. Flag-tagged Pol2 was immunoprecipitated from whole-cell protein extracts, and coprecipitated HA-tagged Dpb2 was examined using western blotting. IP: immunoprecipitation, WCE: whole-cell extracts.

PTI mutation causes genomic instability

To assess the consequences of PTI mutation on genomic stability, we first measured the mutation rate to canavanine resistance in the *pol2-6Δ* strain. Compared to the wild-type strain, there was approximately a seven-fold increase in the mutation rate of Can^R, indicating that PTI mutation exhibits a significant mutator phenotype (Fig. 2A). We then conducted a gross chromosomal rearrangement (GCR) assay to determine if the mutation leads to an increased level of GCR. Our results showed an over 600-fold increase in GCR in the *pol2-6Δ* strain, strongly suggesting that PTI disruption leads to genomic instability (Fig. 2B). Additionally, *pol2-6Δ* exhibited synthetic sickness when combined with rad52 deletion, highlighting the reliance of *pol2-6Δ* on DNA repair mechanisms for optimal growth (Fig. 2C). This suggests that more DNA damage occurs when the PTI is mutated. Furthermore, we mated a series of checkpoint mutants with *pol2-6Δ* to investigate potential genetic interactions. Our results revealed synthetic lethality between *pol2-6Δ* and all tested checkpoint mutants, including *mec1Δ*, *mrc1Δ*, *rad9Δ*, *rad53Δ* (Fig. 2D). This indicates that checkpoint response pathway is required for the survival of *pol2-6Δ*. Based on these find-

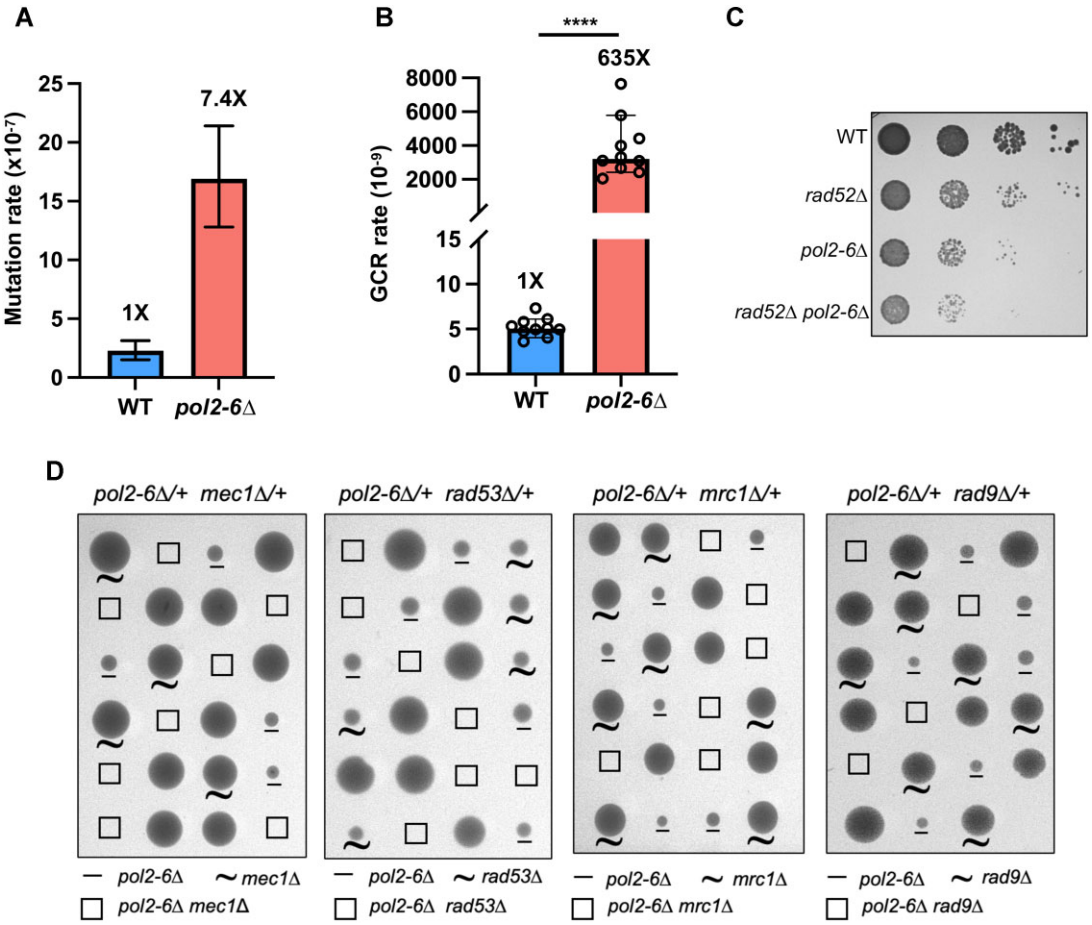

Figure 2. *pol2-6Δ* induces genome instability. (**A**) CAN1 forward mutation rate assay performed in wild-type and *pol2-6Δ* cells at 30°C. Data are presented as mean rates determined from 72 cultures with two biological replicates per genotype. Error bars indicate 95% confidence intervals. (**B**) GCR rate measured in *pol2-6Δ* at 30°C. Data are presented as median rates of 10 cultures from two biological replicates per genotype. Two-tailed Mann–Whitney tests were run for statistical analysis (****$P < 0.0001$). Error bars show 95% confidence intervals. (**C**) Wild-type, *rad52Δ*, *pol2-6Δ*, and *rad52Δ pol2-6Δ* double mutant cells were spotted at 10-fold serial dilutions on YPD medium and incubated at 24°C for 3 days. (**D**) Diploid cells with the indicated genotypes were sporulated, subjected to tetrad analysis on YPD medium, and incubated at 24°C for 3 days.

ings, we conclude that the PTI mutation leads to genomic instability.

PTI point mutant exhibits weaker but similar defects to those of *pol2-6Δ*

Given the severe growth defects associated with *pol2-6Δ*, we aimed to generate a point mutant with improved growth to facilitate further investigation into PTI's function. We created a point mutant, *pol2-6A*, by mutating residues 1131–1136 to alanine. Although this mutant exhibits only a minor growth defect at 30°C, its growth was significantly slower at 37°C (Supplementary Fig. S2A). Like *pol2-6Δ*, the pol2-6A mutation did not affect Pol2 protein levels (Supplementary Fig. S2B). Notably, *pol2-6A* also exhibits a similar level of Can^R mutation rate to *pol2-6Δ* (Supplementary Fig. S2C). Moreover, it also depends on Rad52 for optimal growth (Supplementary Fig. S2D), and shows synthetic sickness with *mec1Δ*, *mrc1Δ*, *rad9Δ*, as well as synthetic lethality with *rad53Δ* (Supplementary Fig. S2E). These results indicate that the point mutant *pol2-6A* shares similar, albeit weaker, defects compared to *pol2-6Δ*. Due to its healthier phenotype, we utilized the *pol2-6A* strain for the remainder of this study for the convenience.

PTI mutation leads to asymmetrical and delayed replication elongation

The observed growth defects and genomic instability in PTI mutants may be attributed to the replication defect of Pol ε. To test this hypothesis, we first examined the cell cycle progression using flow cytometry analysis. Yeast cells were synchronized in the G1 phase and released into S phase, with samples collected from different time points to determine DNA content. We found that *pol2-6A* exhibits delayed S phase progression compared to the wild-type strain, indicating a potential DNA replication defect (Fig. 3A).

To gain further insights into the replication defects in *pol2-6A*, we performed DNA 2D gel analysis to examine the accumulation of replication intermediates at both early (ARS305) and late (ARS1212) origins. Since both origins are located at the center of the assayed DNA fragments, symmetrical bidirectional replication forks primarily generate bubble-shaped replication intermediates, while the accumulation of large Y-shaped intermediates indicates an asymmetrical fork movement (Fig. 3B). In the wild-type strain, a minimal level of Y-shaped replication intermediates, ranging from small to large sizes, is detected at both ARS305 and ARS1212 across time points. These intermediates typically arise from passive replication initiated from neighboring origins. In contrast, beyond

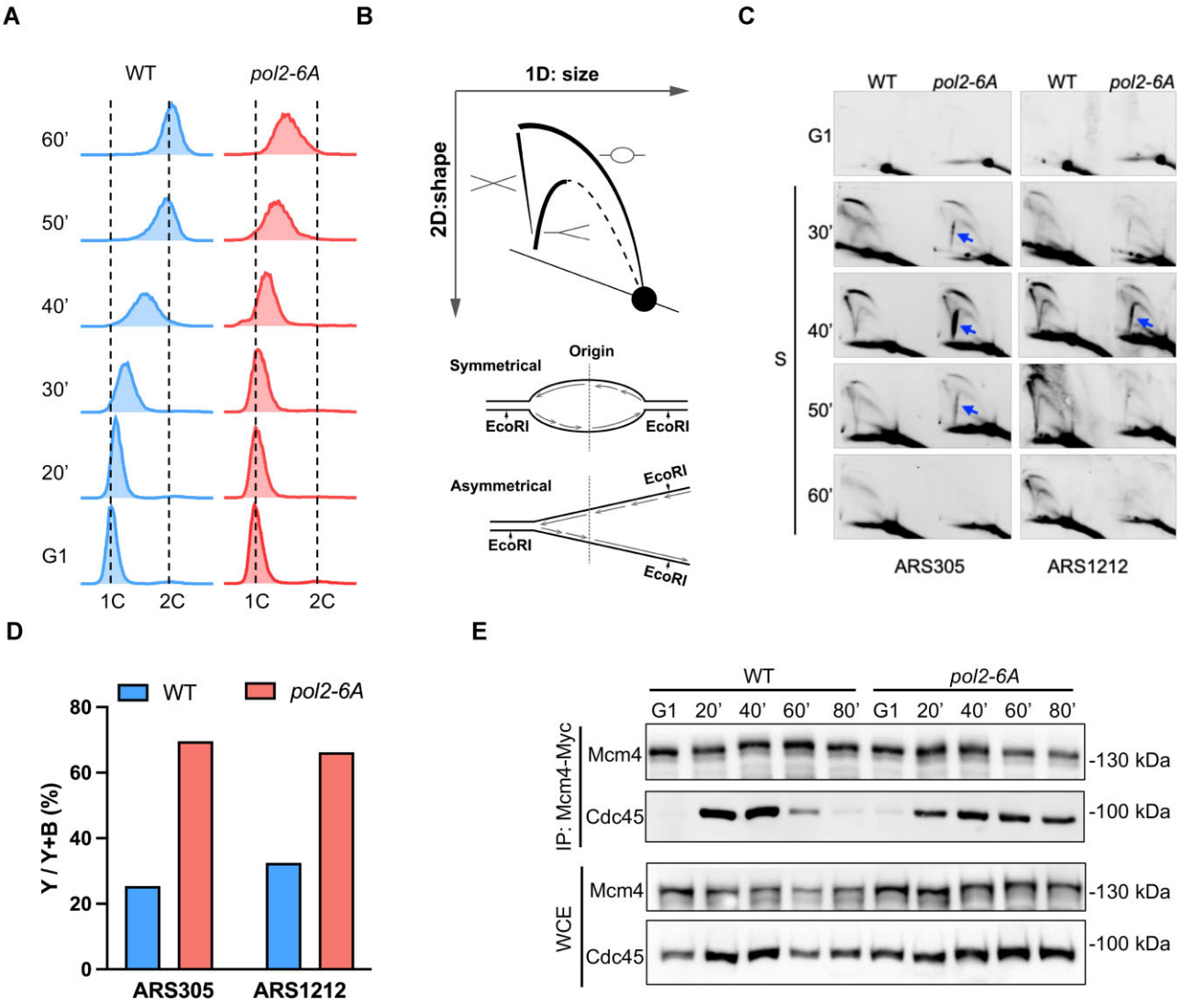

Figure 3. *pol2-6A* delays replication progression. (**A**) Flow cytometry analysis of DNA replication in *pol2-6A* cells. Asynchronous cells were initially arrested at the G1 phase using alpha-factor and subsequently released into the S phase at 24°C. DNA content was measured by flow cytometry. (**B**) Top: Schematic illustrating various forms of replication intermediates (RIs) separated by 2D gel electrophoresis. Bottom: Representation of replication initiation from an origin positioned at the mid-point of a restriction fragment. Symmetric replication yields bubble RIs while asymmetric replication generates Y-shaped RIs. (**C**) 2D gel analysis of replication intermediates in *pol2-6A* compared to wild-type strain. Samples were collected from G1 arrest and release at 24°C, as depicted in the flow cytometry profiles (panel A). Two distinct probes were employed for the specific detection of ARS305 and ARS1212 origins, respectively. (**D**) Quantification of large Y-shaped replication intermediates ratio to total Y- and bubble-shaped intermediates at 40 min (panel C). (**E**) Measurement of CMG levels in *pol2-6A* across S phase. Samples were collected at indicated time points, aligned with the flow cytometry profiles (panel A). Myc-tagged Mcm4 was immunoprecipitated (IP), and the co-purification of Cdc45 was examined. WCE: whole cell extract.

the "background level" of Y-shaped intermediates from passive replication, *pol2-6A* exhibits a high level of large Y-shaped intermediates at both origins (Fig. 3C, indicated by blue arrows). The Y-shaped intermediates peak at 40 min after cells were released into S phase from G1 (Fig. 3C). Quantification showed that the percentage of large Y molecules, relative to the sum of large Y and bubble-shaped intermediates, in *pol2-6A* was approximately three-fold higher (70% versus 25%) at the early origin ARS305 and approximately two-fold higher (66% versus 32%) at the late origin ARS1212 compared to the wild-type strain (Fig. 3D).

Additionally, bubble-shaped replication intermediates emerged at the same timepoint (30 min) in both wild-type and *pol2-6A* strains, with similar levels of replication initiation events (the total amount of bubble-shaped and Y-shaped replication intermediates) (Fig. 3C). These observations suggest that *pol2-6A* does not exhibit an apparent replication initiation defect.

Furthermore, we performed coimmunoprecipitation to assess CMG (Cdc45-MCM-GINS) levels during S phase progression. In the wild-type strain, CMG levels peak at 40 min and then significantly decrease by 60 min, indicating the completion of replication. However, in the *pol2-6A* mutant, CMG levels remain high even at 80 min, suggesting delayed replication (Fig. 3E). This delay likely results from slowed replisome progression caused by the PTI mutation. These findings are consistent with the delayed S phase progression observed in flow cytometry analysis and the accumulation of the Y-shaped

DNA structures in 2D gel analysis. Together, these results suggest that the PTI mutation leads to slowed and asymmetrical replication fork elongation.

Previous studies have indicated that Pol ε acts as a mediator in the activation of DNA replication checkpoint [21, 47, 48]. Consequently, we explored the potential relationship between the PTI insertion and this function. To investigate this, G1-arrested cells were released into hydroxyurea (HU), and samples were collected at various time points for Rad53 western blot analysis (Supplementary Fig. S3). A similar level of phosphorylated Rad53 was observed in both *pol2-6A* mutant and the wild-type strain, suggesting that the *pol2-6A* mutation does not impact the role of Pol ε in replication checkpoint activation.

Mutation in PTI is sensitized by disrupting other replication progression factors

To better understand the role of PTI in DNA replication, we investigated the genetic interactions between the pol2-6A mutation and a series of replication-related mutations. First, we found that *pol2-6A* is synthetically sick with *csm3Δ* and *tof1Δ* mutants under both normal conditions and genotoxic stress (Fig. 4A, Supplementary Fig. S4A and B). Since both proteins are components of the fork protection complex (FPC), and play a key role in positioning the parental DNA duplex for unwinding during DNA replication [20, 49], these data suggest that when parental DNA is not well stabilized for unwinding, *pol2-6A* experiences greater difficulties in DNA replication elongation. Next, we tested the genetic interactions between *pol2-6A* and *dpb3Δ* or *dpb4Δ* mutants, as Dpb3 and Dpb4 are involved in the double-stranded DNA binding and support DNA polymerase's processivity [24, 25]. Both *pol2-6A dpb3Δ* and *pol2-6A dpb4Δ* show much smaller colony sizes on the tetrad dissection plates compared to their single mutant siblings (Fig. 4B). These data suggest that *pol2-6A*'s replication defect is exacerbated when the polymerase becomes less processive due to relaxed binding to double-stranded DNA.

Given that the previously reported POPS mutant exhibits a defect in replication progression [33, 34], we explored the potential relationships between the PTI and POPS mutations. We found that combining the PTI mutation (pol2-6A) with POPS mutation (pol2-R567C) results in an additive effect on cell growth, suggesting that the POPS and PTI domains function non-redundantly (Fig. 4C). Since POPS mutations show significant synthetic sickness with the PIP mutation (PIPm, F1199A and F1200A) [34], which impairs the Polε–PCNA interaction [37], we tested the impact of the PIP mutation on *pol2-6A*. Cells with both the PIP mutation and the pol2-6A mutation exhibit worse growth compared to single mutants at 30°C or higher temperatures (Fig. 4D). However, the impact of PIP mutation on pol2-6A is not as severe as on the POPS mutation. Since the replication elongation defect caused by the POPS mutation can be rescued by inactivating the exonuclease activity of Pol2, which protects the 3′end of the nascent strand from degradation [34], we investigated whether a similar scenario occurs in *pol2-6A*. However, the catalytic dead mutation (exo$^-$, D290A E292A) of the Pol2 exonuclease domain does not rescue the growth defect of *pol2-6A* (Fig. 4E). In sum, our results suggest that the PTI insertion supports replication progression through a different mechanism than the POPS domain.

Additionally, we tested the genetic interplay between *pol2-6A* and mutations in other proteins related to replication progression. One such protein is Rrm3, a 5′ to 3′ DNA helicase that removes proteins bound at pause sites, such as those in rDNA tandem repeats, facilitating the replisome's movement past non-histone protein-DNA complexes [50]. Another is RNase H2, which plays a crucial role in resolving R-loops generated by replication-transcription conflicts [51]. In both cases, while the double mutants *pol2-6A rrm3Δ* and *pol2-6A rnh201Δ* showed minimal growth defects compared to single mutants at 30°C, slower growth was observed at higher temperature (34°C and 37°C) (Fig. 4F and G). Additionally, *pol2-6A rrm3Δ* exhibits greater sensitivity to genotoxic stress at 30°C compared to single mutants, whereas *pol2-6A rnh201Δ* does not (Supplementary Fig. S4A, Supplementary Fig. S4C).

Taken together, by investigating the genetic interactions of *pol2-6A* with a series of mutations related to DNA replication elongation, we conclude that the PTI insertion likely supports the processivity of Pol ε rather than protecting nascent strand 3′ end, especially when replisome encounters obstacles.

Pol ε^{6A} exhibits impaired DNA synthesis *in vitro*

To investigate the specific function of the PTI insertion in replication progression, we purified wild-type Pol ε (Pol ε^{WT}) and its mutated form, Pol ε^{6A} (Supplementary Fig. S5A). The integrity of the purified Pol ε^{6A} protein further confirmed that the PTI mutations do not affect the stability or composition of Pol ε. We then conducted *in vitro* assays to assess their polymerase and exonuclease activities, following established protocols [45, 46].

In the polymerase assay, a 5′ fluorescently labeled 50-nt primer annealed to an 80-nt template was used as the DNA substrate. Equal amounts of Pol ε^{WT} and Pol ε^{6A} were tested for the primer extension activity. Pol ε^{6A} exhibited reduced polymerase activity compared to the wild-type protein (Fig. 5A). Specifically, after a 10-min reaction, the wild-type protein converted ∼83% of the substrate into the product, whereas the mutated protein converted around 57% (Fig. 5B). We also assessed the exonuclease activity of Pol ε^{6A} in a similar reaction by omitting dNTPs. Monitoring the degradation of the 5′ fluorescently labeled 50-nt strand revealed reduced exonuclease activity of Pol ε^{6A} (Fig. 5C). After a 10-min reaction, less than 10% of substrate remained intact with Pol ε^{WT}, while more than 30% of the substrate remained undigested with Pol ε^{6A} (Fig. 5D). These results indicate that the PTI insertion is crucial for supporting both the polymerase and exonuclease activities of Pol ε.

Next, we sought to determine whether the DNA polymerase activity of Pol ε^{6A} was compromised on long, natural templates in a reaction supplemented with or without PCNA, using a modified version of previously described protocols [29, 46]. We purified three additional protein complexes required in this system: PCNA, RFC and RPA (Supplementary Fig. S4B). PCNA was loaded onto a singly primed, 7.25-kb circular M13 single-stranded DNA template, and the replication reaction was initiated by adding either Pol ε^{WT} or Pol ε^{6A} proteins (Fig. 5E). In the absence of PCNA, Pol ε^{WT} generated short DNA products in a time-dependent manner (Fig. 5F, lanes 1–3). After 15 min, the average product size was smaller than the 564-nt marker, consistent with previous reports [29]. In contrast, Pol ε^{6A} produced significantly fewer and shorter products under the same conditions (Fig. 5F, lanes 4–6), indicat-

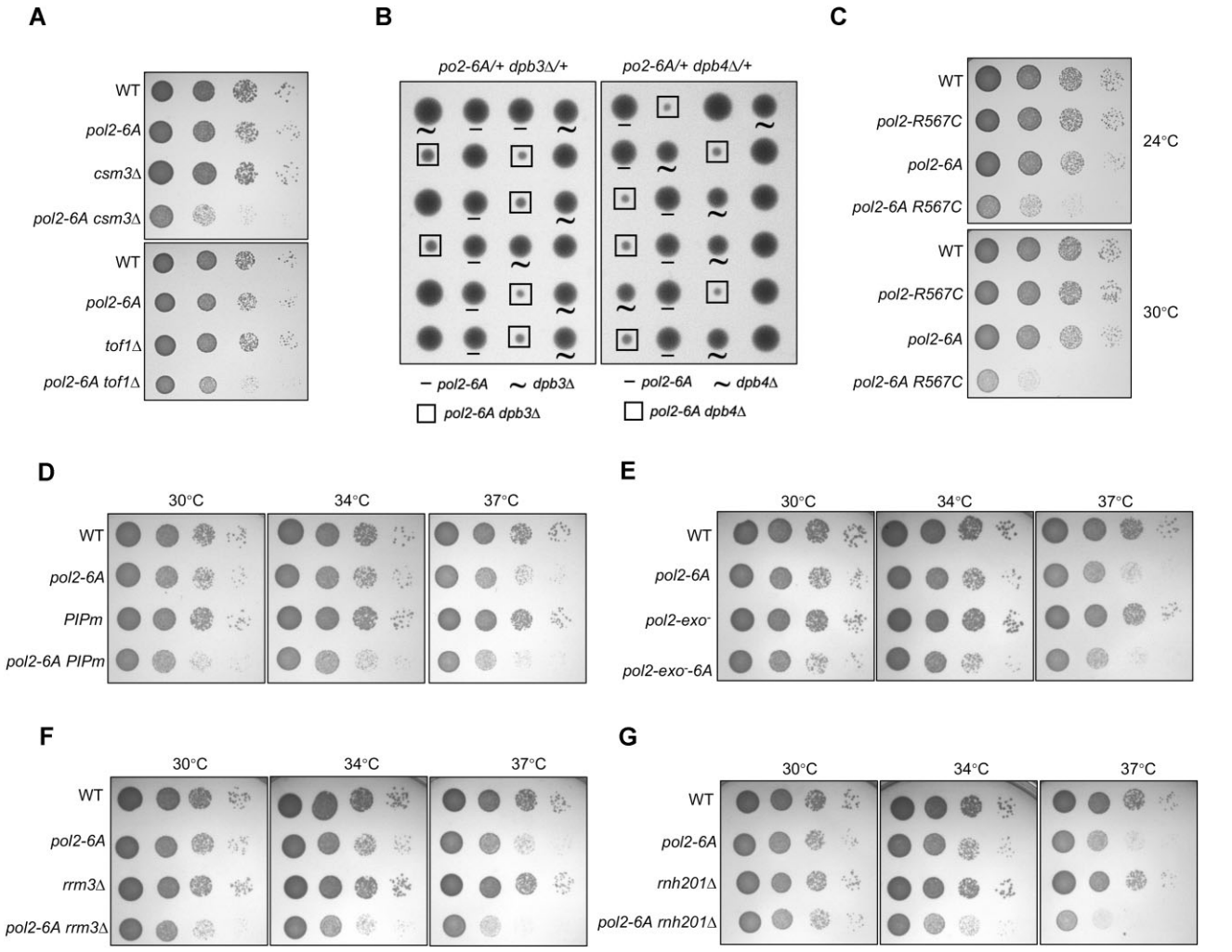

Figure 4. Mutations in replication progression-related factors sensitize *pol2-6A*. (**A**) Cells of *pol2-6A csm3Δ*, *pol2-6A tof1Δ* double mutants, and related single mutant cells were spotted at 10-fold serial dilutions on YPD medium and then incubated at 30°C for 2 days. (**B**) Heterozygous diploid cells of *pol2-6A dpb3Δ* and *pol2-6A dpb4Δ* were sporulated, subjected to tetrad analysis on YPD medium, and subsequently incubated at 30°C for 3 days. (**C**) Cells of *pol2-6A R567C* double mutants and related single mutant cells were spotted at 10-fold serial dilutions on YPD medium and incubated at both 24°C and 30°C for 2 days. (D-G) Double mutants of *pol2-6A PIPm*, *pol2-exo⁻-6A*, *pol2-6A rrm3Δ*, and *pol2-6A rnh201Δ*, along with related single mutants were spotted at 10-fold serial dilutions on YPD medium and then incubated at 30°C, 34°C, and 37°C for 2 days.

ing a severe impairment in DNA polymerase activity on long substrates due to the PTI mutation. In the presence of PCNA, Pol ε^{WT} synthesized much longer DNA products, achieving full-length replication within 15 min (Fig. 5F, lanes 7–9), illustrating the processivity enhancement provided by PCNA. While PCNA also improved Pol ε^{6A}'s processivity, the yield of DNA products was markedly lower, and full-length products were barely detectable (Fig. 5F, lanes 10–12). These results underscore the importance of the PTI insertion in the processive DNA polymerase activity of Pol ε. Given that recent cryo-EM structures of the human Pol ε-PCNA complex identified the PTI insertion as an interacting region with PCNA [11, 36], we cannot rule out the possibility that the Pol2-6A mutation might also affect the interaction between Pol ε and PCNA in budding yeast.

In summary, our *in vitro* assays with short oligonucleotide templates and long circular templates demonstrate that the PTI mutation directly impairs the DNA synthesis of Pol ε. Further studies are needed to determine whether the PTI mutation also influences replication processivity by altering the Pol ε–PCNA interaction.

Pol ε^{6A} exhibits reduced processivity *in vitro*

Given that the PTI insertion is located peripherally to the catalytic domain (Fig. 1A) [9, 10], the pol2-6A mutation likely does not directly affect the catalytic site of the polymerase domain. We hypothesized that the reduced DNA synthesis observed with Pol ε^{6A} might result from the impaired processivity. To test this, we analyzed the processivity of Pol ε under single-hit conditions by lowering the enzyme-to-substrate ratio [52, 53]. Initial assays with short templates (Fig. 5A–D) used an enzyme-to-substrate ratio of 1:5, allowing multiple turnovers and thus did not isolate processivity defects. We adjusted the enzyme-to-substate ratio to 1:10 and 1:30 to establish single-hit conditions, as described previously [53]. Under these conditions, Polε^{6A} exhibited reduced polymerase and exonuclease activities compared to Pol ε^{WT} (Fig. 6A–H), suggesting that its processivity is compromised when PTI is disrupted. Conversely, at a 1:1 enzyme-to-substrate ratio, no significant difference in polymerase activity was observed between Pol ε^{WT} and Pol ε^{6A}, although the exonuclease activity of Pol ε^{6A} remained lower (Fig. 6I–L). This likely reflects

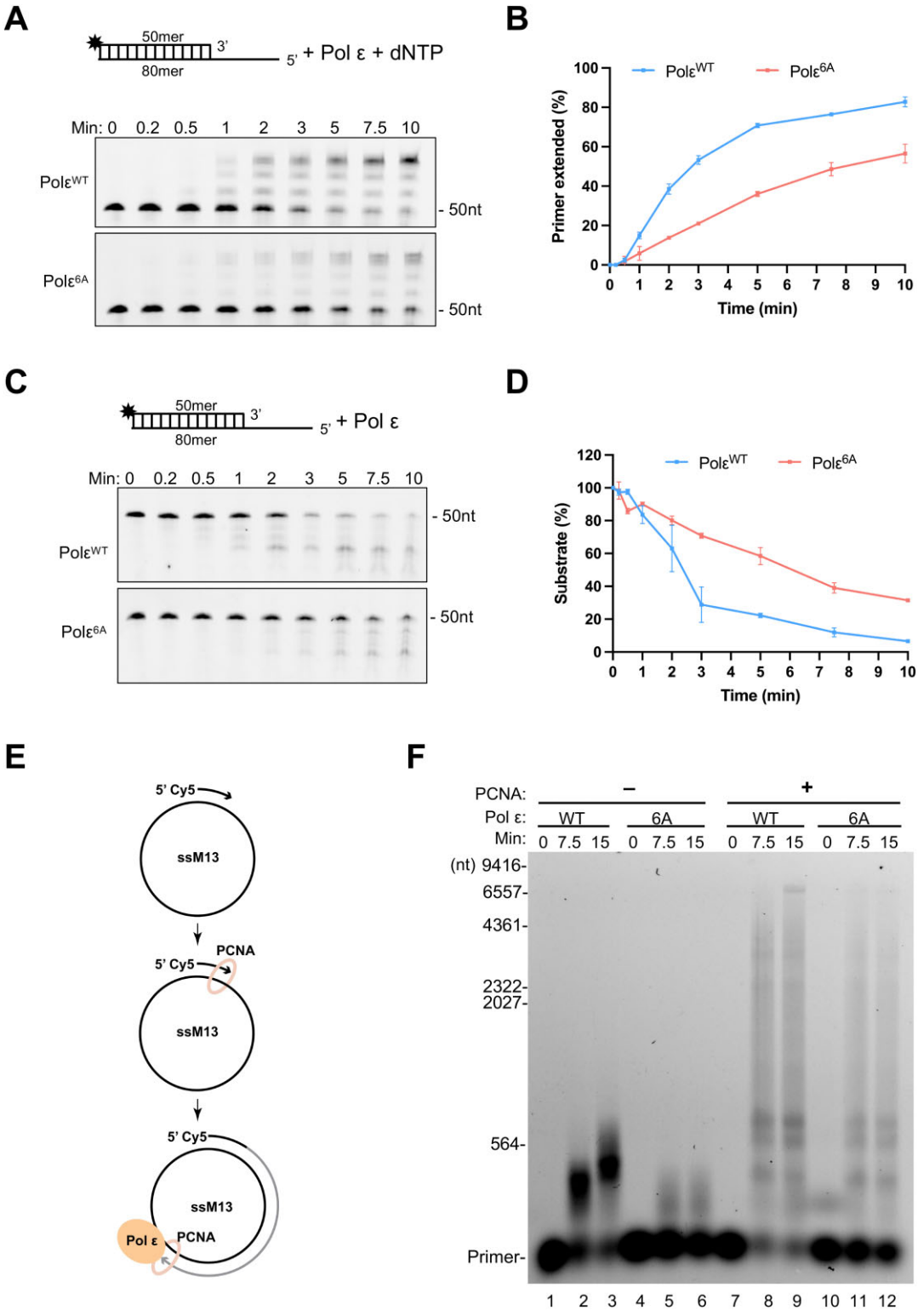

Figure 5. Pol ε^{6A} exhibits reduced polymerase and exonuclease activity *in vitro*. (**A**) Polymerase activity of Pol ε^{WT} and Pol ε^{6A} was assayed using a 25 nM substrate comprising a 50-nt primer labeled with 5′FAM annealed to an 80nt template and 5 nM polymerase. Reaction progress was monitored at specified time points using 10% denaturing polyacrylamide gel containing 8 M urea. (**B**) Quantification of polymerase activity. Ratio of the product signal to the total signal of the substrate and product from the gel in panel A was determined. Mean values were derived from two independent experiments. Error bars represent the standard deviation. (**C**) Exonuclease activity of Pol ε^{WT} and Pol ε^{6A} was assayed using a 25 nM substrate comprising a 50-nt primer labeled with 5′FAM annealed to an 80-nt template and 5 nM polymerase. Experiments were conducted similarly to panel A, with the exclusion of dNTPs from the reaction mixture. (**D**) Quantification of exonuclease activity. Determination of the remaining substrate at each time point from the gel in panel C. The substrate amount at time point "0" was set as 100%. Mean values were derived from two independent experiments. Error bars represent the standard deviation. (**E**) Schematic of DNA polymerase assay using the long template M13mp18 in the presence of PCNA. (**F**) The polymerase activity of Pol ε^{WT} and Pol ε^{6A} were assayed using a single-stranded M13mp18 template annealed with a 5′ Cy5 labeled primer. The assay included 3.75 nM Pol ε, with or without 37.5 nM PCNA. The products were separated in a 0.8% alkaline agarose gel.

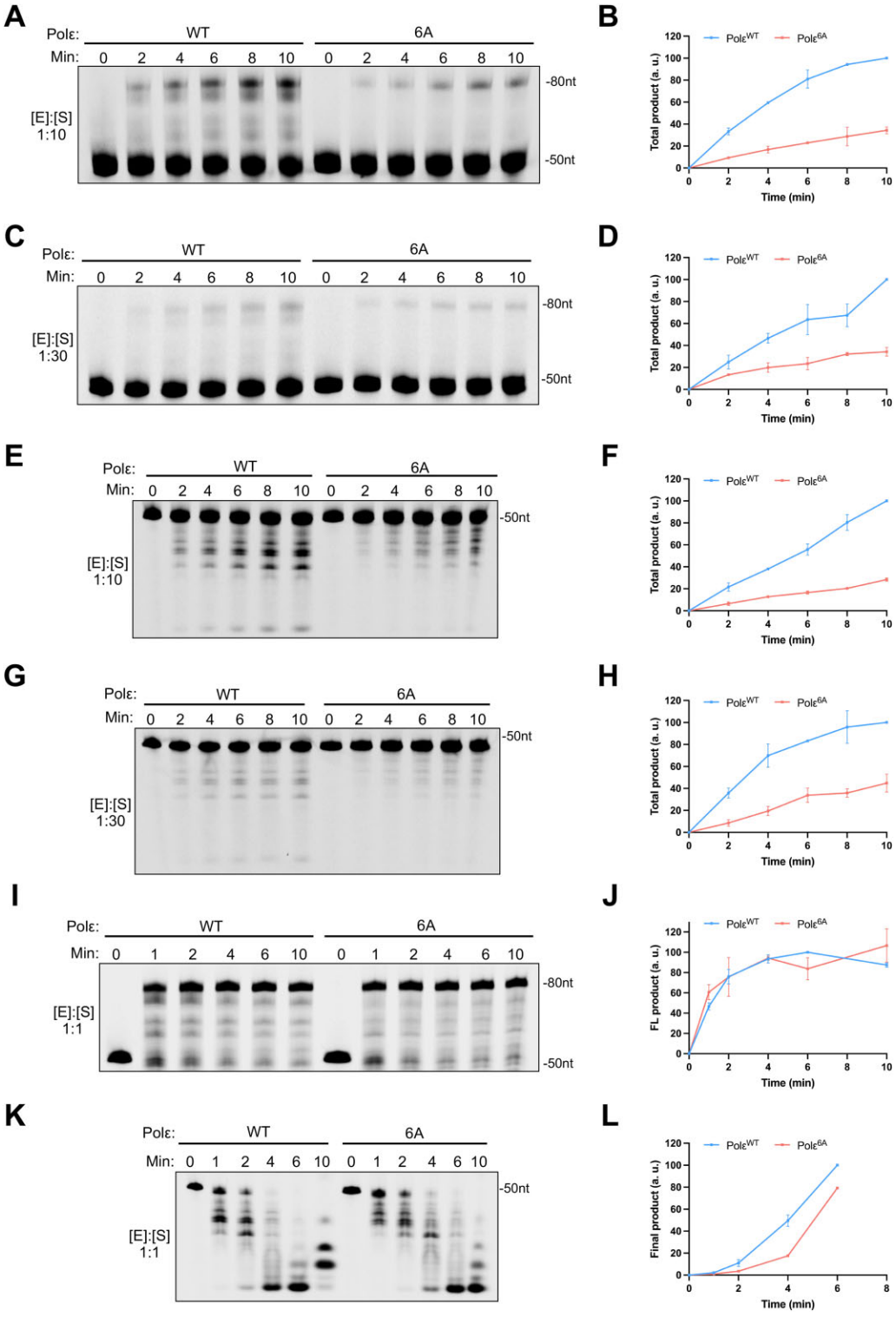

Figure 6. Pol ε^{6A} exhibits reduced processivity *in vitro*. (**A**) Polymerase activity of Pol ε^{WT} and Polε^{6A} was analyzed using a 30 nM DNA substrate comprising a 50-nt primer labeled with 5′Cy5 annealed to an 80-nt template. Reactions were conducted with 3 nM polymerase, and the product formation was monitored at indicated time points using 10% denaturing polyacrylamide gel containing 8 M urea. (**B**) Quantification of the total product (all product bands combined) at each time point from the gel in panel A. The highest amount in the wild-type sample was set to 100. (**C**) Polymerase activity of Pol ε^{WT} and Polε^{6A} was analyzed as in panel A, except with 1 nM polymerase. (**D**) Quantification of the total product at each time point from the gel in panel C. (**E**) Exonuclease activity of Pol ε^{WT} and Pol ε^{6A} was assessed under conditions similar to panel A, but without dNTPs. (**F**) Quantification of the total product at each time point from the gel in panel E. (**G**) Exonuclease activity of Pol ε^{WT} and Pol ε^{6A} was assessed under conditions similar to panel C, but without dNTPs. (**H**) Quantification of the total product at each time point from the gel in panel G. (**I**) Polymerase activity of Pol ε^{WT} and Polε^{6A} was analyzed as in panel A, using 30 nM polymerase. (**J**) Quantification of the full-length product (the highest band) at each time point from the gel in panel I. (**K**) Exonuclease activity of Pol ε^{WT} and Pol ε^{6A} was evaluated as in panel E, using 30 nM polymerase, and omitting dNTPs. (**L**) Quantification of the final product (lowest band in the gel) at each time point from the gel in panel K. For all quantifications, mean values were derived from two independent experiments, and error bars represent the standard deviation.

multiple enzyme turnovers on the DNA substrate, which compensates for the reduced processivity of Pol ε^{6A}. In conclusion, these results demonstrate that the PTI insertion is critical for maintaining the processivity of Pol ε during DNA synthesis.

Pol ε^{6A} exhibits compromised DNA binding *in vitro*

To understand how the PTI mutation affects the processivity of Pol ε, we examined its DNA binding activity. The thumb domain of DNA polymerases is known to play a crucial role in DNA binding [9, 10]. We hypothesized that the PTI insertion within the thumb domain might contributes to the ability of Pol ε to stably interact with DNA substrates. To test this hypothesis, we conducted an electrophoretic mobility shift assay (EMSA) using the same short substrate used in the *in vitro* polymerase activity assay. The EMSA results showed a significant reduction in the proportion of shifted substrate with Pol ε^{6A} compared to the wild-type protein (Fig. 7A and B). These data suggest that the PTI insertion facilitates Pol ε binding to DNA substrates. Consequently, when this region is mutated, Pol ε exhibits reduced affinity for the substrate, leading to a decrease in processivity.

Discussion

Distinct structural features differentiate Pol ε from other replicative polymerases. The Pol2C, P domain, and POPS domain all contribute to various aspects of the functions of Pol ε [9, 11, 19, 20, 33, 36]. In this study, we carefully examined a previously uncharacterized structural insertion—the PTI insertion in Pol2—and revealed its critical role in DNA replication. By creating a series of deletion mutations within the PTI insertion, we pinpointed six key amino acid residues crucial for PTI's function and cell growth (Fig. 1). Deletion or mutation of these residues led to an increased mutation rate and GCR, a heightened reliance on the DNA repair protein Rad52, and on proteins involved in DNA damage checkpoint pathways (Mec1, Mrc1, Rad9, and Rad53) (Fig. 2). These findings suggest that disruption of PTI leads to genomic instability. Moreover, we found that the PTI mutants exhibit defects in replication progression, which likely underlie the observed growth defect and genomic instability.

Our study provides three lines of evidence to support the role of PTI in replication progression. First, genetic interaction analysis shows that the PTI mutation is sensitized by mutations in replication progression factors, including Csm3, Tof1, PCNA, Dpb3/4, Rrm3, and RNase H2, indicating that PTI plays a role in replication progression (Fig. 4). Second, *in vivo* detection of accumulation of large Y-shaped replication intermediates and the prolonged presence of the CMG complex during S phase progression indicate asymmetrical fork movement and delayed replication progression (Fig. 3). Finally, *in vitro* polymerase assays and EMSA using purified proteins reveal that the PTI mutation reduces DNA binding and decreases processivity (Figs 5–7). Thus, we conclude that the PTI domain significantly contributes to replication progression.

Although the previously reported POPS domain also supports efficient replication progression [33, 34], our findings suggest that the PTI domain facilitates DNA replication progression differently. We observed synthetic sickness between POPS and PTI mutations, indicating that these domains promote replication progression through distinct mechanisms (Fig. 4C). Additionally, there are key differences between the two types of mutants. First, the PTI mutant exhibits a sevenfold increase in the mutation rate (Fig. 2A, Supplementary Fig. S2C), whereas the POPS mutant's mutation rate is similar to that of the wild-type strain [33]. This difference is likely due to lower DNA binding affinity of Pol ε in the PTI mutant, which reduces its exonuclease activity. Second, the PTI mutation is more sensitive to the mutations in the replisome components, such as fork protection complex, which stabilizes CMG on DNA, rather than to mutations in proteins required to remove replication barriers, such as RNase H2 and Rrm3 (Fig. 4A, F, and G). In contrast, the POPS mutation is highly sensitive to the latter mutations because the POPS domain primarily curbs the exonuclease activity when the replication fork movement slows upon encountering replication barriers [33]. Moreover, the growth defect of the POPS mutant can be partially rescued by the catalytic dead mutation in the Pol2 exonuclease domain [34], which is not the case for the PTI mutant (Fig. 4E). These data suggest that Pol ε employs different unique domains to maintain efficient DNA synthesis through distinct mechanisms: the POPS domain primarily prevents degradation of the 3′ end of the nascent DNA, while the PTI domain promotes the binding of Pol ε to the DNA substrate.

How does PTI support replication progression? PTI is located far from the catalytic site of the polymerase domain (Fig. 1A), making it unlikely to directly modulate the catalytic site for DNA synthesis. One possibility is that PTI is required for the thumb domain to form an appropriate structural conformation with high affinity for the DNA substrate. When the PTI insertion is disrupted, the thumb domain may adopt a different conformation with lower DNA binding affinity. Since Pol3, the catalytic subunit of Pol δ, which lacks the PTI insertion, still forms a similar structure to Pol2N (Fig. 1A), we speculate that the conformational change caused by PTI disruption is likely subtle. A previous study has shown that Pol δ has much lower DNA binding affinity compared to Pol ε [29], and PTI may contribute to this discrepancy. Another unique domain of Pol ε, the P domain, has been shown to promote high processivity of Pol ε through enhanced binding to double-stranded DNA [9]. Therefore, the mechanism by which PTI supports tight DNA binding to promote the processivity of Pol ε is somewhat similar to that of the P domain. In contrast to the wild-type, the PTI mutant has relaxed DNA binding, which could cause Pol2N to frequently dissociate from the substrate, leading to low processivity (Fig. 7C).

During the preparation of this manuscript, cryo-EM structures of human Pol ε-PCNA complex were reported, revealing three interfaces between these two proteins [11, 36]. The major interface is mediated by the PIP motif, consistent with previous data in budding yeast [31, 37, 54]. In contrast, the PTI insertion forms a much smaller interface with one of the PCNA protomers. However, no functional analyses of this interaction have been conducted in either budding yeast or humans, leaving its role in supporting the processivity of Pol ε unclear.

To investigate the PTI-PCNA interface, we superimposed the yeast Pol2N structure onto the human POLE-PCNA complex. This comparison revealed that while the overall fold of the PTI insertions is conserved between yeast and humans there is a slight structural shift between the two PTIs (Supplementary Fig. S6A). Sequence alignment of residues at the human PTI-PCNA interface identified only two conserved residues in the yeast PTI (R1124 and D1129) (Supplementary Fig. S6B). Notably, these residues were not included among

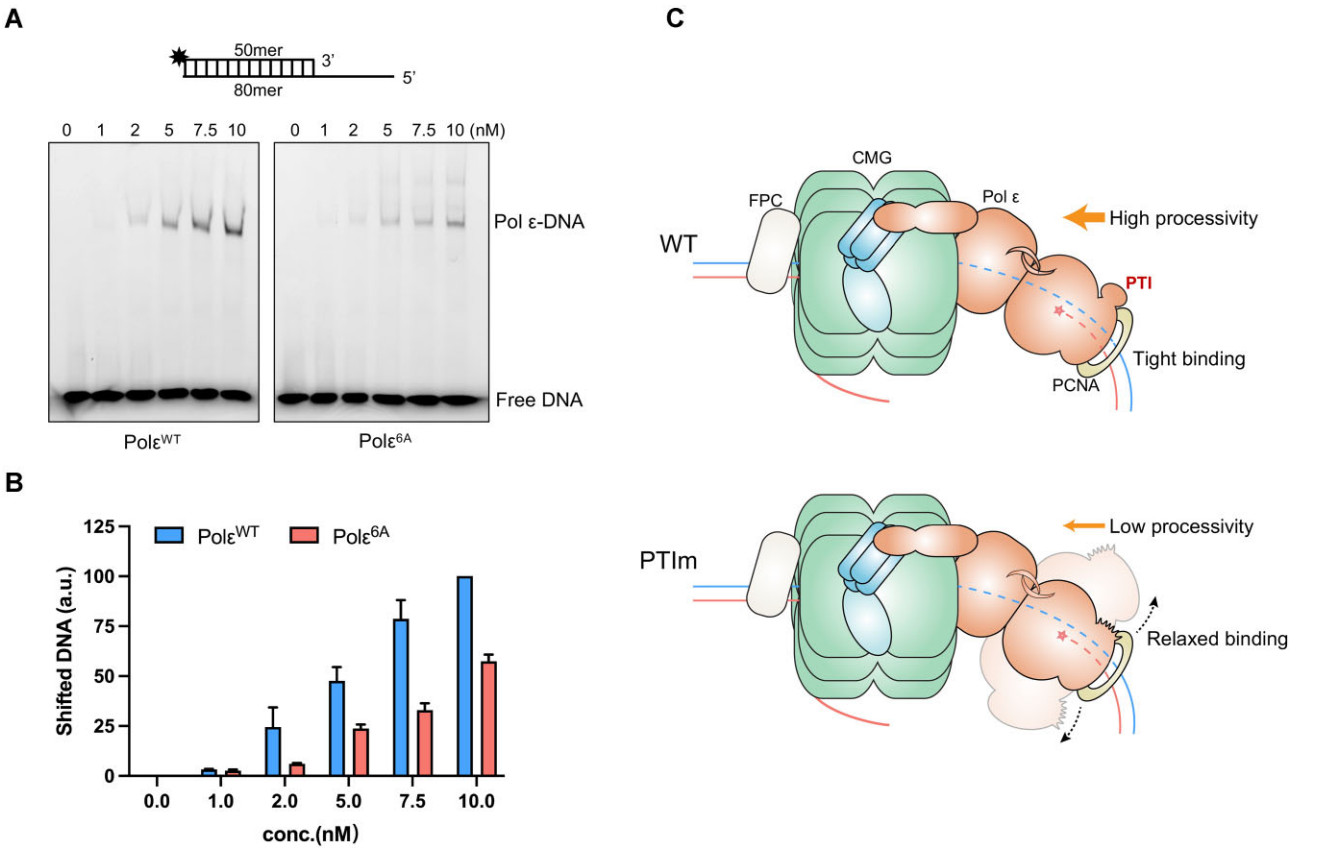

Figure 7. Pol ε^{6A} exhibits reduced DNA binding activity *in vitro*. (**A**) EMSA evaluating the DNA binding activity of Pol ε^{WT} and Pol ε^{6A}. 5′-FAM-labeled DNA substrates, identical to those used in Fig. 5A, were incubated with increasing concentrations of Pol ε^{WT} or Pol ε^{6A}. Protein–DNA complexes were resolved by 4% polyacrylamide gel electrophoresis (PAGE). (**B**) Quantification of shifted DNA percentage at different protein concentrations. The highest amount in the wild-type sample was set to 100. Mean values were derived from two independent experiments. Error bars represent the standard deviation. (**C**) A proposed model illustrating how PTI supports processive replication elongation by supporting stable DNA binding.

the six mutated residues in the *pol2-6A* strain. To explore the functional significance of the PTI-PCNA interface residues, we generated a double mutant (R1124A, D1129A) and a composite mutant that also included alanine substitutions at the yeast counterparts of non-conserved human PTI-PCNA interface residues (R1124A, D1129A, L1128A, P1130A, and S1131A). Neither mutant strain exhibited growth defects or sensitivity to MMS (Supplementary Fig. S6C). In contrast, the *pol2-PIPm* mutant displayed MMS sensitivity. These results suggest that the PTI–PCNA interaction is less critical than the canonical PIP–PCNA interaction. Furthermore, compared to the *pol2-PIPm* mutant, the *pol2-6A* mutant showed more pronounced growth defects and MMS sensitivity (Fig. 4D, Supplementary Fig. S6C). This indicates that the PTI's role extends beyond its interaction with PCNA and directly modulating the intrinsic processivity of Pol ε.

Moreover, DNA replication processivity appears to rely on PCNA differently in budding yeast and humans. Yeast cells with PIP mutations grow normally like the wild-type (Fig. 4D) [37], and *in vitro* replication assays show that PCNA is only required for optimal leading strand replication [30, 31]. In contrast, human Pol ε relies heavily on PCNA for leading strand synthesis [32]. Therefore, although Pol ε and PCNA are conserved between yeast and humans, their specific functions in DNA replication progression may differ. The interfaces captured in the human Pol ε-PCNA structures may not necessarily reflect the situation in yeast cells. Further functional analyses of the interactions between Pol ε and PCNA in yeast and humans will help to clarify these differences.

Acknowledgements

We thank Dr. Ping Xu and Dr. Xiaolan Zhao for critical reading the manuscript and providing valuable comments, and thank Dr. Xiaolan Zhao, Dr. Bingbing Wan, Dr. Lei Wei, and Dr. Fei Tao for providing us with strains and plasmids.

Author contributions: X.M. conceived the study. X.M., S.A., and S.Z. designed the experiments. S.A. and S.Z. performed the experiments. X.M., S.A., and S.Z. analyzed the data. X.M. wrote the manuscript with review and editing from S.A. and S.Z.

Supplementary data

Supplementary data is available at NAR online.

Conflict of interest

The authors have no conflicts of interest to declare.

Funding

National Key Research and Development Program of China (2023YFA0913700) and National Natural Science Founda-

tion of China (32370072). Funding to pay the Open Access publication charges for this article was provided by National Key Research and Development Program of China (2023YFA0913700) and National Natural Science Foundation of China (32370072).

Data availability

The data underlying this article are available in the article and in its online supplementary material.

References

1. Burgers PMJ, Kunkel TA. Eukaryotic DNA replication fork. *Annu Rev Biochem* 2017;**86**:417–38. https://doi.org/10.1146/annurev-biochem-061516-044709
2. Pellegrini L, Costa A. New insights into the mechanism of DNA duplication by the eukaryotic replisome. *Trends Biochem Sci* 2016;**41**:859–71. https://doi.org/10.1016/j.tibs.2016.07.011
3. Fukui T, Yamauchi K, Muroya T *et al.* Distinct roles of DNA polymerases delta and epsilon at the replication fork in Xenopus egg extracts. *Genes Cells* 2004;**9**:179–91. https://doi.org/10.1111/j.1356-9597.2004.00716.x
4. Pursell ZF, Isoz I, Lundström E-B *et al.* Yeast DNA polymerase ε participates in leading-strand DNA replication. *Science* 2007;**317**:127–30. https://doi.org/10.1126/science.1144067
5. Nick McElhinny SA, Gordenin DA, Stith CM *et al.* Division of labor at the eukaryotic replication fork. *Mol Cell* 2008;**30**:137–44. https://doi.org/10.1016/j.molcel.2008.02.022
6. Morrison A, Araki H, Clark AB *et al.* A third essential DNA polymerase in *S. cerevisiae*.. *Cell* 1990;**62**:1143–51. https://doi.org/10.1016/0092-8674(90)90391-Q
7. Chilkova O, Jonsson BH, Johansson E. The quaternary structure of DNA polymerase epsilon from *Saccharomyces cerevisiae*. *J Biol Chem* 2003;**278**:14082–6. https://doi.org/10.1074/jbc.M211818200
8. Yuan Z, Georgescu R, Schauer GD *et al.* Structure of the polymerase epsilon holoenzyme and atomic model of the leading strand replisome. *Nat Commun* 2020;**11**:3156. https://doi.org/10.1038/s41467-020-16910-5
9. Hogg M, Osterman P, Bylund GO *et al.* Structural basis for processive DNA synthesis by yeast DNA polymerase epsilon. *Nat Struct Mol Biol* 2014;**21**:49–55. https://doi.org/10.1038/nsmb.2712
10. Jain R, Rajashankar KR, Buku A *et al.* Crystal structure of yeast DNA polymerase epsilon catalytic domain. *PLoS One* 2014;**9**:e94835. https://doi.org/10.1371/journal.pone.0094835
11. Roske JJ, Yeeles JTP. Structural basis for processive daughter-strand synthesis and proofreading by the human leading-strand DNA polymerase Pol epsilon. *Nat Struct Mol Biol* 2024;**12**:1921–31. https://doi.org/10.1038/s41594-024-01370-y
12. Kesti T, Flick K, Keränen S *et al.* DNA polymerase ε catalytic domains are dispensable for DNA replication, DNA repair, and cell viability. *Mol Cell* 1999;**3**:679–85. https://doi.org/10.1016/S1097-2765(00)80361-5
13. Dua R, Levy DL, Campbell JL. Analysis of the essential functions of the C-terminal protein/protein interaction domain of *Saccharomyces cerevisiae* pol ε and its unexpected ability to support growth in the absence of the DNA polymerase domain*. *J Biol Chem* 1999;**274**:22283–8. https://doi.org/10.1074/jbc.274.32.22283
14. Garbacz MA, Lujan SA, Burkholder AB *et al.* Evidence that DNA polymerase delta contributes to initiating leading strand DNA replication in *Saccharomyces cerevisiae*. *Nat Commun* 2018;**9**:858. https://doi.org/10.1038/s41467-018-03270-4
15. Tahirov TH, Makarova KS, Rogozin IB *et al.* Evolution of DNA polymerases: an inactivated polymerase-exonuclease module in Pol epsilon and a chimeric origin of eukaryotic polymerases from two classes of archaeal ancestors. *Biol Direct* 2009;**4**:11. https://doi.org/10.1186/1745-6150-4-11
16. Muramatsu S, Hirai K, Tak YS *et al.* CDK-dependent complex formation between replication proteins Dpb11, Sld2, pol epsilon, and GINS in budding yeast. *Genes Dev* 2010;**24**:602–12. https://doi.org/10.1101/gad.1883410
17. Handa T, Kanke M, Takahashi TS *et al.* DNA polymerization-independent functions of DNA polymerase epsilon in assembly and progression of the replisome in fission yeast. *MBoC* 2012;**23**:3240–53. https://doi.org/10.1091/mbc.e12-05-0339
18. Sengupta S, van Deursen F, de Piccoli G *et al.* Dpb2 integrates the leading-strand DNA polymerase into the eukaryotic replisome. *Curr Biol* 2013;**23**:543–52. https://doi.org/10.1016/j.cub.2013.02.011
19. Goswami P, Abid Ali F, Douglas ME *et al.* Structure of DNA-CMG-Pol epsilon elucidates the roles of the non-catalytic polymerase modules in the eukaryotic replisome. *Nat Commun* 2018;**9**:5061. https://doi.org/10.1038/s41467-018-07417-1
20. Xu Z, Feng J, Yu D *et al.* Synergism between CMG helicase and leading strand DNA polymerase at replication fork. *Nat Commun* 2023;**14**:5849. https://doi.org/10.1038/s41467-023-41506-0
21. Navas TA, Zhou Z, Elledge SJ. DNA polymerase epsilon links the DNA replication machinery to the S phase checkpoint. *Cell* 1995;**80**:29–39. https://doi.org/10.1016/0092-8674(95)90448-4
22. Dua R, Levy DL, Campbell JL. Role of the putative zinc finger domain of *Saccharomyces cerevisiae* DNA polymerase epsilon in DNA replication and the S/M checkpoint pathway. *J Biol Chem* 1998;**273**:30046–55. https://doi.org/10.1074/jbc.273.45.30046
23. Yu C, Gan H, Serra-Cardona A *et al.* A mechanism for preventing asymmetric histone segregation onto replicating DNA strands. *Science* 2018;**361**:1386–9. https://doi.org/10.1126/science.aat8849
24. Tsubota T, Maki S, Kubota H *et al.* Double-stranded DNA binding properties of *Saccharomyces cerevisiae* DNA polymerase ϵ and of the Dpb3p-Dpb4p subassembly. *Genes Cells* 2003;**8**:873–88. https://doi.org/10.1046/j.1365-2443.2003.00683.x
25. Aksenova A, Volkov K, Maceluch J *et al.* Mismatch repair-independent increase in spontaneous mutagenesis in yeast lacking non-essential subunits of DNA polymerase epsilon. *PLoS Genet* 2010;**6**:e1001209. https://doi.org/10.1371/journal.pgen.1001209
26. Georgescu RE, Langston L, Yao NY *et al.* Mechanism of asymmetric polymerase assembly at the eukaryotic replication fork. *Nat Struct Mol Biol* 2014;**21**:664–70. https://doi.org/10.1038/nsmb.2851
27. Lancey C, Tehseen M, Raducanu VS *et al.* Structure of the processive human Pol delta holoenzyme. *Nat Commun* 2020;**11**:1109. https://doi.org/10.1038/s41467-020-14898-6
28. Zheng F, Georgescu RE, Li H *et al.* Structure of eukaryotic DNA polymerase delta bound to the PCNA clamp while encircling DNA. *Proc Natl Acad Sci USA* 2020;**117**:30344–53. https://doi.org/10.1073/pnas.2017637117
29. Chilkova O, Stenlund P, Isoz I *et al.* The eukaryotic leading and lagging strand DNA polymerases are loaded onto primer-ends via separate mechanisms but have comparable processivity in the presence of PCNA. *Nucleic Acids Res* 2007;**35**:6588–97. https://doi.org/10.1093/nar/gkm741
30. Yeeles JTP, Janska A, Early A *et al.* How the eukaryotic replisome achieves rapid and efficient DNA replication. *Mol Cell* 2017;**65**:105–16. https://doi.org/10.1016/j.molcel.2016.11.017
31. Aria V, Yeeles JTP. Mechanism of bidirectional leading-strand synthesis establishment at eukaryotic DNA replication origins. *Mol Cell* 2019;**73**:199–211. https://doi.org/10.1016/j.molcel.2018.10.019
32. Baris Y, Taylor MRG, Aria V *et al.* Fast and efficient DNA replication with purified human proteins. *Nature* 2022;**606**:204–10. https://doi.org/10.1038/s41586-022-04759-1
33. Meng X, Wei L, Devbhandari S *et al.* DNA polymerase epsilon relies on a unique domain for efficient replisome assembly and

strand synthesis. *Nat Commun* 2020;**11**:204–10. https://doi.org/10.1038/s41467-020-16095-x
34. Meng X, Claussin C, Regan-Mochrie G *et al.* Balancing act of a leading strand DNA polymerase-specific domain and its exonuclease domain promotes genome-wide sister replication fork symmetry. *Genes Dev* 2023;**37**:74–9. https://doi.org/10.1101/gad.350054.122
35. Meng X, Wei L, Peng XP *et al.* Sumoylation of the DNA polymerase epsilon by the Smc5/6 complex contributes to DNA replication. *PLoS Genet* 2019;**15**:e1008426. https://doi.org/10.1371/journal.pgen.1008426
36. He Q, Wang F, Yao NY *et al.* Structures of the human leading strand polε–PCNA holoenzyme. *Nat Commun* 2024;**15**:7874. https://doi.org/10.1038/s41467-024-52257-x
37. Dua R, Levy DL, Li CM *et al.* In vivo reconstitution of *Saccharomyces cerevisiae* DNA polymerase epsilon in insect cells. Purification and characterization. *J Biol Chem* 2002;**277**:7889–96. https://doi.org/10.1074/jbc.M108546200
38. Zhao XL, Blobel G. A SUMO ligase is part of a nuclear multiprotein complex that affects DNA repair and chromosomal organization. *Proc Natl Acad Sci USA* 2005;**102**:4777–82. https://doi.org/10.1073/pnas.0500537102
39. Putnam CD, Kolodner RD. Determination of gross chromosomal rearrangement rates. *Cold Spring Harb Protoc* 2010;**2010**:pdb.prot5492. https://doi.org/10.1101/pdb.prot5492
40. Wan B, Wu J, Meng X *et al.* Molecular basis for control of diverse genome stability factors by the multi-BRCT scaffold Rtt107. *Mol Cell* 2019;**75**:238–51. https://doi.org/10.1016/j.molcel.2019.05.035
41. Lang GI. Measuring mutation rates using the Luria-Delbruck fluctuation assay. *Methods Mol Biol* 2018;**1672**:21–31. https://doi.org/10.1007/978-1-4939-7306-4_3
42. Lopes M, Cotta-Ramusino C, Liberi G *et al.* Branch migrating sister chromatid junctions form at replication origins through Rad51/Rad52-independent mechanisms. *Mol Cell* 2003;**12**:1499–510. https://doi.org/10.1016/S1097-2765(03)00473-8
43. Devbhandari S, Jiang J, Kumar C *et al.* Chromatin constrains the initiation and elongation of DNA replication. *Mol Cell* 2017;**65**:131–41. https://doi.org/10.1016/j.molcel.2016.10.035
44. He Z, Wong JS, Maniar HS *et al.* Assessing the requirements for nucleotide excision repair proteins of *Saccharomyces cerevisiae* in an *in vitro* system*. *J Biol Chem* 1996;**271**:28243–9. https://doi.org/10.1074/jbc.271.45.28243
45. Barbari SR, Beach AK, Markgren JG *et al.* Enhanced polymerase activity permits efficient synthesis by cancer-associated DNA polymerase ϵ variants at low dNTP levels. *Nucleic Acids Res* 2022;**50**:8023–40. https://doi.org/10.1093/nar/gkac602
46. Xing X, Kane DP, Bulock CR *et al.* A recurrent cancer-associated substitution in DNA polymerase epsilon produces a hyperactive enzyme. *Nat Commun* 2019;**10**:374. https://doi.org/10.1038/s41467-018-08145-2
47. Lou H, Komata M, Katou Y *et al.* Mrc1 and DNA polymerase epsilon function together in linking DNA replication and the S phase checkpoint. *Mol Cell* 2008;**32**:106–17. https://doi.org/10.1016/j.molcel.2008.08.020
48. Pardo B, Crabbe L, Pasero P. Signaling pathways of replication stress in yeast. *FEMS Yeast Res* 2017;**17**:fow101. https://doi.org/10.1093/femsyr/fow101
49. Baretic D, Jenkyn-Bedford M, Aria V *et al.* Cryo-EM structure of the fork protection complex bound to CMG at a replication fork. *Mol Cell* 2020;**78**:926–40. https://doi.org/10.1016/j.molcel.2020.04.012
50. Ivessa AS, Lenzmeier BA, Bessler JB *et al.* The *Saccharomyces cerevisiae* helicase Rrm3p facilitates replication past nonhistone protein-DNA complexes. *Mol Cell* 2003;**12**:1525–36. https://doi.org/10.1016/S1097-2765(03)00456-8
51. Cerritelli SM, Crouch RJ. Ribonuclease H: the enzymes in eukaryotes. *FEBS J* 2009;**276**:1494–505. https://doi.org/10.1111/j.1742-4658.2009.06908.x
52. Bambara RA, Fay PJ, Mallaber LM. Methods of analyzing processivity. In: *Methods in Enzymology*. Vol: **262**. San Diego, CA, USA: Academic Press, 1995, 270–80. https://doi.org/10.1016/0076-6879(95)62023-0
53. Asturias FJ, Cheung IK, Sabouri N *et al.* Structure of *Saccharomyces cerevisiae* DNA polymerase epsilon by cryo-electron microscopy. *Nat Struct Mol Biol* 2006;**13**:35–43. https://doi.org/10.1038/nsmb1040
54. Devbhandari S, Remus D. Rad53 limits CMG helicase uncoupling from DNA synthesis at replication forks. *Nat Struct Mol Biol* 2020;**27**:461–71. https://doi.org/10.1038/s41594-020-0407-7

Received: September 14, 2024. **Revised:** February 20, 2025. **Editorial Decision:** February 24, 2025. **Accepted:** February 26, 2025